Journal of Cranio-Maxillo-Facial Surgery xxx (xxxx) xxx

Contents lists available at ScienceDirect

Journal of Cranio-Maxillo-Facial Surgery

journal homepage: www.jcmfs.com

Cone beam CT for the assessment of bone microstructure to predict head shape changes after spring-assisted craniosynostosis surgery

Tanya Wolffenbuttel [a,b,d,*], Sara Ajami [a,b], Alessandro Borghi [a,b,c], Silvia Schievano [a,b], David Dunaway [a,b], Noor ul Owase Jeelani [a,b], Maarten Koudstaal [d]

[a] Craniofacial Unit, Great Ormond Street Hospital for Children, London, UK
[b] Great Ormond Street Institute of Child Health, University College London, London, UK
[c] Department of Engineering, Durham University, Durham, UK
[d] Department of Oral and Maxillofacial Surgery, Erasmus Medical Centre, Rotterdam, the Netherlands

ARTICLE INFO

Keywords:
Craniosynostosis
Spring-assisted cranioplasty
Preoperative planning
Cranial bone microstructure
Cone beam CT

ABSTRACT

Head shape changes following spring-cranioplasty for craniosynostosis (CS) can be difficult to predict. While previous research has indicated a connection between surgical outcomes and calvarial bone microstructure ex-vivo, there exists a demand for identifying imaging biomarkers that can be translated into clinical settings and assist in predicting these outcomes. In this study, ten parietal (8 males, age 157 ± 26 days) and two occipital samples (males, age 1066 and 1162 days) were collected from CS patients who underwent spring cranioplasty procedures. Samples' microstructure were examined using clinical imaging modalities (dental CBCT, C-arm CT) and micro-CT. Cranial index (CI) was measured to evaluate patients' head shape before and after surgery, with an investigation into their relationship with morphometric measurements. Bone cross-sectional thickness (CsTh) showed significant correlation to CI increase post-SAC for C-arm CT ($\rho = -0.857$, $p = 0.014$) and 8.9 μm micro-CT ($\rho = -0.857$, $p = 0.014$). In addition, bone volume (BV) was correlated to CI increase for CBCT ($\rho = -0.643$, $p = 0.013$), 50 μm micro-CT ($\rho = -0.857$, $p < 0.001$) and 90 μm micro-CT ($\rho = -0.679$, $p = 0.008$). High correlation with micro-CT resampled to match respective voxel sizes was demonstrated for both CBCT and C-arm CT measurements of CsTh and BV ($\rho \geq 0.860$, $p < 0.001$). This preliminary study demonstrates the potential of clinical CT devices to aid in pre-surgical decision making in CS.

1. Introduction

Multiple surgical techniques are employed globally to treat craniosynostosis (CS), yet a unanimous consensus remains elusive regarding the optimal timing and method for intervention. Minimally invasive surgical approaches to treat CS such as spring-assisted cranioplasty (SAC) and endoscopic approaches offer numerous benefits including a reduction of perioperative blood loss, dimensions of surgical incisions, total operative time and hospital stay compared to more invasive procedures (Breakey et al., 2021; Rodgers et al., 2017). At Great Ormond Street Hospital for Children (GOSH) in London, SAC has become the preferred operative technique for isolated sagittal CS, while spring-assisted posterior vault expansion (SA-PVE) is used to treat multi-sutural and syndromic CS in patients with a brachycephalic head shape or ICP-related concerns. However, given the unpredictable nature of head shape changes post spring-assisted CS surgery, secondary calvarial remodelling may be required to address unsatisfactory aesthetic outcomes or concerns of raised intracranial pressure. The documented surgical revision rates of 13% for SA-PVE (Breakey et al., 2021) and 20% for SAC (Rodgers et al., 2017) procedures highlight the need for identifying biomarkers that can aid in predicting head shape outcomes post spring-assisted surgery for CS.

One of the factors that plays an important role in head shape changes after surgical treatment is bone microstructure (Rodriguez-Florez et al., 2017). After birth, the paediatric skull is made up of one-layered cancellous tissue that is well-suited to accommodate the growing brain. During the first year of life calvarial bone evolves to a trilaminar, sandwich-like structure consisting of two external cortical tables and a central trabecular layer (the diploë) through the process of intramembranous ossification, as shown in Fig. 1. Rodriguez-Florez et al. reported that extent of head shape changes following SAC was associated with the variation in parietal bone microstructure, and the

* Corresponding author. Craniofacial Unit, Great Ormond Street Hospital for Children, London, WC1N 3JH, UK.
E-mail address: tanya.wolffenbuttel@outlook.com (T. Wolffenbuttel).

https://doi.org/10.1016/j.jcms.2024.11.014
Received 1 July 2024; Received in revised form 10 October 2024; Accepted 15 November 2024

effectiveness of the surgery was related to the degree of development of a trilaminar structure and bone thickness in calvarium. It is hypothesized that unilaminar bone is more malleable and thus associated with bigger changes in cephalic index (CI) after mechanical spring distraction. For patients with a unilaminar structure of the parietal bone, average skull thickness was below 2 mm and the improvement in CI was greatest. In contrast, patients with a skull thickness above 3 mm experienced less than 4% improvement in CI. Development of the skull to a trilaminar structure takes place at a certain point during the first year of life, but the exact age varies. This corresponds to the finding that among infants aged 3–8 months, age at SAC is, in contrast to bone microstructure, not significantly correlated with changes in CI (Rodriguez-Florez et al., 2017). Thus, pre-operative analysis of cranial bone microstructure should be considered to predict head shape changes following SAC.

The gold standard to determine bone microstructure is micro-computed tomography (micro-CT) imaging. However, micro-CT imaging is not suitable for use in clinical settings due to its high radiation dose, limited field of view and long scanning time. Hence, there is an unmet need for imaging biomarkers that can reliably be leveraged in clinical imaging modalities (Ajami et al., 2022). The development of advanced CT imaging techniques such as cone beam CT (CBCT), C-arm CT, multi-slice CT (MSCT) and high-resolution peripheral quantitative CT (HR-pQCT) allows for the assessment of bone quality at the three-dimensional (3D) microstructure level. However, use of MSCT and HR-pQCT for evaluation of bone quality is limited due to its relatively high radiation dose and exclusive scanning of non-central sites, respectively (Manske et al., 2010; Wang et al., 2022; Guha et al., 2020; Donnelly, 2011).

CBCT imaging presents several advantages regarding radiation dose, cost effectiveness, scanning time and space requirements compared to other potential imaging modalities. The lowest obtainable voxel size with a commercial CBCT device is currently 75 μm. A variety of human and animal bones have previously been scanned with CBCT devices to assess its ability to depict bone microstructure, including mandibular, maxillary, tibial and trapezial bone (Guha et al., 2020; Ibrahim et al., 2014, 2021; Kim et al., 2015; Klintström et al., 2014, 2016; Kulah et al., 2019; Mys et al., 2018, 2021; Van Dessel et al., 2013, 2016, 2017; Parsa et al., 2015). Dach et al. investigated the effect of different CBCT voxel sizes and acquisition times on linear deviation figures in a marcerated human skull (Dach et al., 2018). However, morphometric measurements of the skull on a trabecular level using CBCT has not yet been investigated. C-arm CT devices integrate a cone beam X-ray source and flat panel detector within C-arm gantry, permitting its use in theatre settings. Three-dimensional data can be obtained in a single rotation of the gantry. This imaging technique is frequently used for interventional procedures and can achieve a voxel size of 50 μm (Orth et al., 2008). The aim of this study is to assess the reliability of available clinical imaging modalities, such as CBCT and C-arm CT, to determine calvarial bone microstructure compared to the gold standard micro-CT, and to identify an imaging biomarker that is predictive of SAC in the treatment of sagittal CS.

2. Materials and methods

2.1. Sample collection and preparation

At GOSH, cranial bone fragments are routinely removed along the fused suture during SAC and SA-PVE and usually discarded (Breakey et al., 2021; Rodgers et al., 2017). Following ethical approval and parental consent (REC reference 09/H0722/28), 10 parietal and 2 occipital bone samples were collected, cleaned of soft tissue, wrapped in a phosphate-buffered saline (PBS) soaked gauze and stored at −20 °C. Prior to scanning, samples were defrosted for a minimum of 3 h at room temperature, while still covered by PBS-soaked gauze. Samples were then fixed in 10% neutral buffered formalin (NBF) solution for 24 h and subsequently stored in PBS with sodium azide.

2.2. Measurement of head shape

Pre- and postoperative images were retrieved from the GOSH electronic database to determine CI (biparietal diameter (BPD)/occipitofrontal diameter (OFD) x 100), which serves as an indicator of head shape changes (Fig. 2). Preoperative images were either conventional X-rays (n = 7) or CT scans (n = 5) of the skull, with the latter being performed for preoperative planning in more complicated cases. Postoperatively, all patients underwent conventional X-ray imaging of the skull.

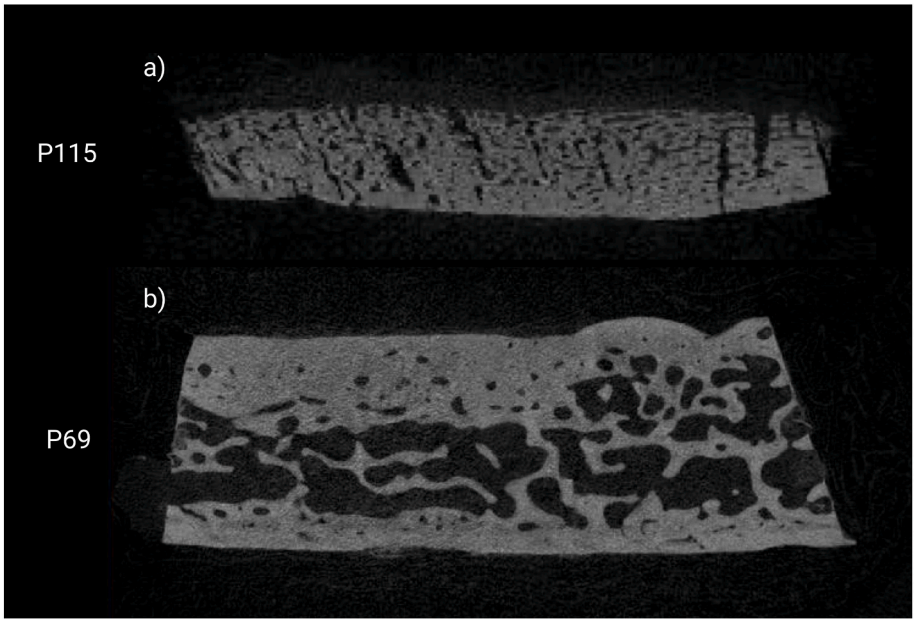

Fig. 1. Micro-CT cross-sections of (a) P115 with a unilaminar structure; (b) P69 with a trilaminar structure, consisting of two cortical layers with diploë cavity in between.

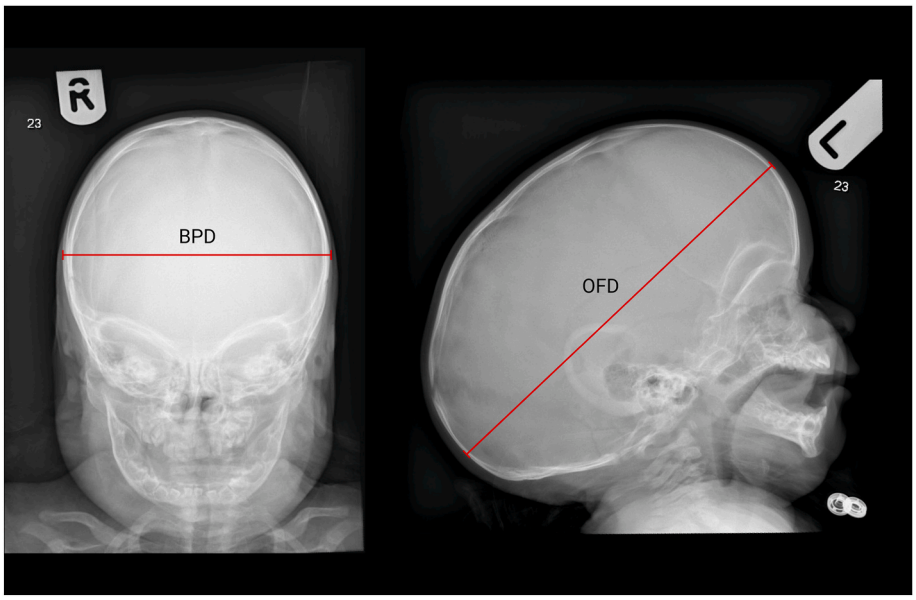

Fig. 2. Cephalic index measurement on a pre-operative X-ray of a scaphocephalic patient. BPD and OFD were measured to include calvarial bone diameter.

2.3. Image acquisition

Samples were scanned with the micro-CT Bruker Skyscan 1172 (SkyScan, Kontich, Belgium). Scan parameters were set at a voxel size of 8.9 µm, X-ray tube voltage of 49 kV, tube current of 200 µA, 590 ms exposure time, 0.5 mm aluminium filter, rotation step of 0.40, average framing 2 and random movement 10. In addition, Dental CBCT images were obtained using the Carestream 9300 scanner (Carestream Health, New York, USA). Scan parameters were set at a voxel size of 90 µm, slice thickness of 90 µm, X-ray tube voltage of 90 kV, tube current of 5 µA and an exposure time of 20 s. C-arm CT images were obtained with the Artis Zee C-arm (Siemens AG, Forchheim, Germany) at a voxel size of 50 µm and slice thickness of 100 µm. The X-ray tube voltage was set at 109 kV, tube current 212 mA and an exposure time of 18 s. To avoid movement artefacts and sample dehydration during image acquisition, samples were stabilized using cling film.

2.4. Image reconstruction, registration and analysis

Dental CBCT and C-arm CT DICOM datasets were transformed from 16-bit to 8-bit and converted to BMP files using ImageJ 1.53q. C-arm CT images were reconstructed in Syngo X Workplace using the preset mode 'DynaCT Head' at a slice matrix of 512 x 512 pixels. Micro-CT images were reconstructed using NRecon 1.7.1.0 (Skyscan, Kontich, Belgium).

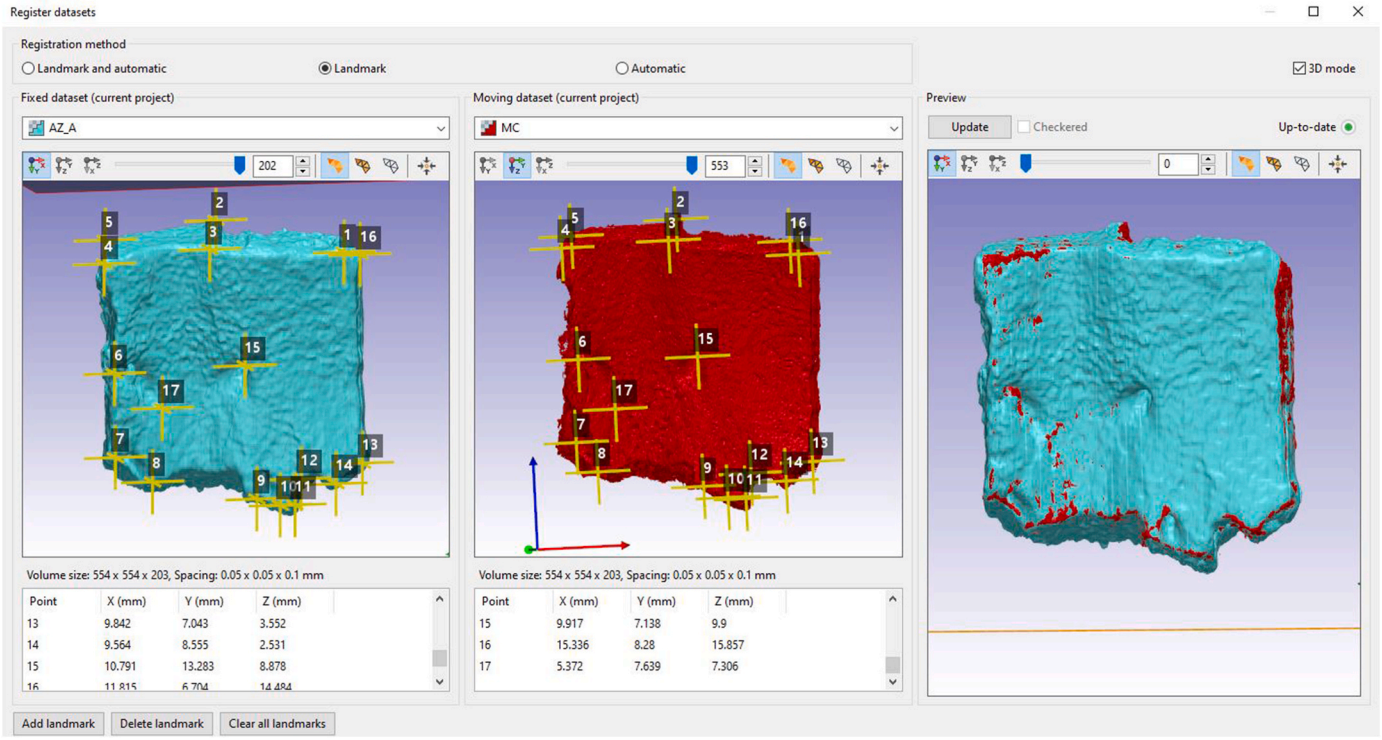

Fig. 3. Registration of dental CBCT and C-arm CT images to micro-CT using manual landmarking.

In Simpleware ScanIP O-2018, micro-CT images were resampled to match the voxel size of dental CBCT and C-arm CT datasets: 90 and 50 μm, respectively. Thereafter, dental CBCT and C-arm CT images were manually registered to micro-CT images in Simpleware ScanIP using landmark references (Fig. 3). For each sample, two regions of interest (ROI) measuring 3 × 3 mm were randomly selected at a distance up to 2 mm away from the cranial suture. To enhance image contrast, the unsharp mask filter was applied to dental CBCT and C-arm CT datasets in ImageJ at a mask weight of 0.60 and radius of 1.0 and 3.0 pixels, respectively.

Lastly, CT Analyser 1.20.8.0 (Skyscan, Kontich, Belgium) was used to perform morphological analysis. Grey value thresholds for image segmentation were operator-selected. Measured structural parameters for all samples were total bone volume (BV; mm^3), bone volume fraction (BV/TV; %), total bone surface (BS; mm^2), specific bone surface (BS/BV; mm^{-1}), total porosity percentage (Po; %) and cross-sectional thickness (CsTh; μm). An overview of image processing is given in Fig. 4.

2.5. Statistical analysis

Statistical analyses were performed using IBM SPSS Statistics 28.0 (SPSS, Inc., Chicago, Il, USA). The assumption of normal distribution of the data was examined and rejected based on the Shapiro-Wilk test. Median values [IQR] are reported, unless indicated otherwise. Statistically significant differences between measurements were assessed using the Wilcoxon signed-rank test for non-parametric paired measurements. Correlations were assessed using Spearman's rank correlation coefficient. Inter-imaging agreement was displayed using Bland-Altman plots (Bland and Altman, 1995). The alpha level of significance for all analyses was set at 0.05. Measures of statistical confidence are reported as two-tailed p-values.

3. Results

3.1. Characteristics of bone samples

In the present study 12 samples representing a trilaminar bone structure were collected from paediatric patients, surgically treated for CS at GOSH between November 2019 and May 2022. A total of 10 parietal bone samples were collected after SAC from patients affected by non-syndromic, isolated sagittal CS (8 males and 2 females, age at surgery = 157 ± 26 days, ranging between 118 and 190 days). In addition, 2 occipital samples were included from patients affected by syndromic, multi-sutural CS who underwent SA-PVE (both males, age at surgery = 1066 and 1162 days, syndromic diagnosis of Sotos and Crouzon, respectively) (Fig. 5). Sample dimensions ranged between 5.7 and 15.0 mm in the axis perpendicular to the fused suture and 8.7–19.2 mm parallel to the fused suture.

3.2. Micro-CT measurements (voxel size 8.9 μm)

Sample characteristics were determined with micro-CT imaging at a voxel size of 8.9 μm. Median values for $BV_{\mu CT}$, $BV/TV_{\mu CT}$, $BS_{\mu CT}$, $BS/BV_{\mu CT}$, $Po_{\mu CT}$ and $CsTh_{\mu CT}$ were 13.33 mm^3 [4.51], 60.12% [13.15], 223.78 mm^2 [48.41], 15.64 mm^{-1} [6.89], 39.89% [13.16] and 1348 μm [183], respectively (Fig. 6). Bone samples with an increased $CsTh_{\mu CT}$ were significantly associated with increasing $BV_{\mu CT}$ ($\rho = 0.846$, $p < 0.001$) and decreasing $BS/BV_{\mu CT}$ ($\rho = -0.678$, $p = 0.015$). In addition, $BV_{\mu CT}$ was negatively correlated with $BS/BV_{\mu CT}$ ($\rho = -0.685$, $p = 0.014$).

3.3. Dental CBCT measurements (voxel size 90 μm)

The root mean standard error (RMSE) of dental CBCT registration versus resampled micro-CT images (90 μm) was 0.2074 ± 0.0569 mm. The RMSE and lower grey value threshold for image segmentation per sample (range; 140–185) are noted in the appendix.

Significant differences were found between dental CBCT and 90 μm micro-CT BS and BS/BV measurements ($p = 0.001$). For the other morphometric measures of interest, no significant differences between dental CBCT and 90 μm micro-CT values were found (Table 1). All dental CBCT measurements were significantly correlated to 90 μm micro-CT measurements ($p \leq 0.05$) (Fig. 7). Strong correlations were found for BV_{CBCT} ($\rho = 0.972$, $p < 0.001$) and $CsTh_{CBCT}$ ($\rho = 0.951$, $p < 0.001$). In addition, moderate to strong correlations were found for BS_{CBCT} ($\rho = 0.713$, $p = 0.009$) and BS/BV_{CBCT} ($\rho = 0.594$, $p = 0.042$). Bland-Altman analysis showed a bias of 0.28 mm^3 between BV_{CBCT} and $BV_{\mu CT90}$ with

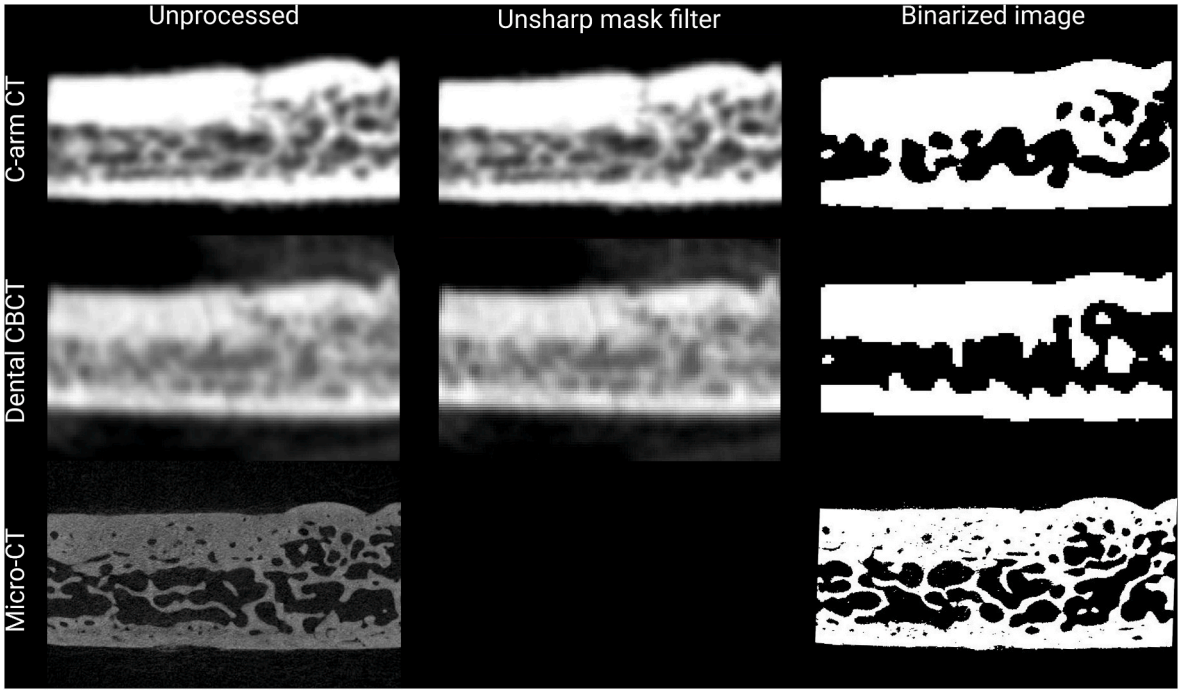

Fig. 4. Overview of image processing steps before calculation of morphometric parameters.

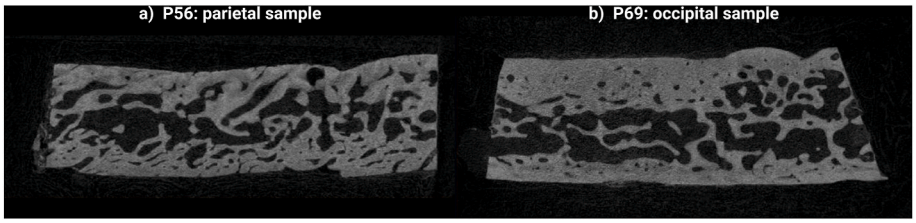

Fig. 5. Micro-CT images at a voxel size of 8.9 μm of trilaminar structure in (a) parietal bone and (b) occipital bone.

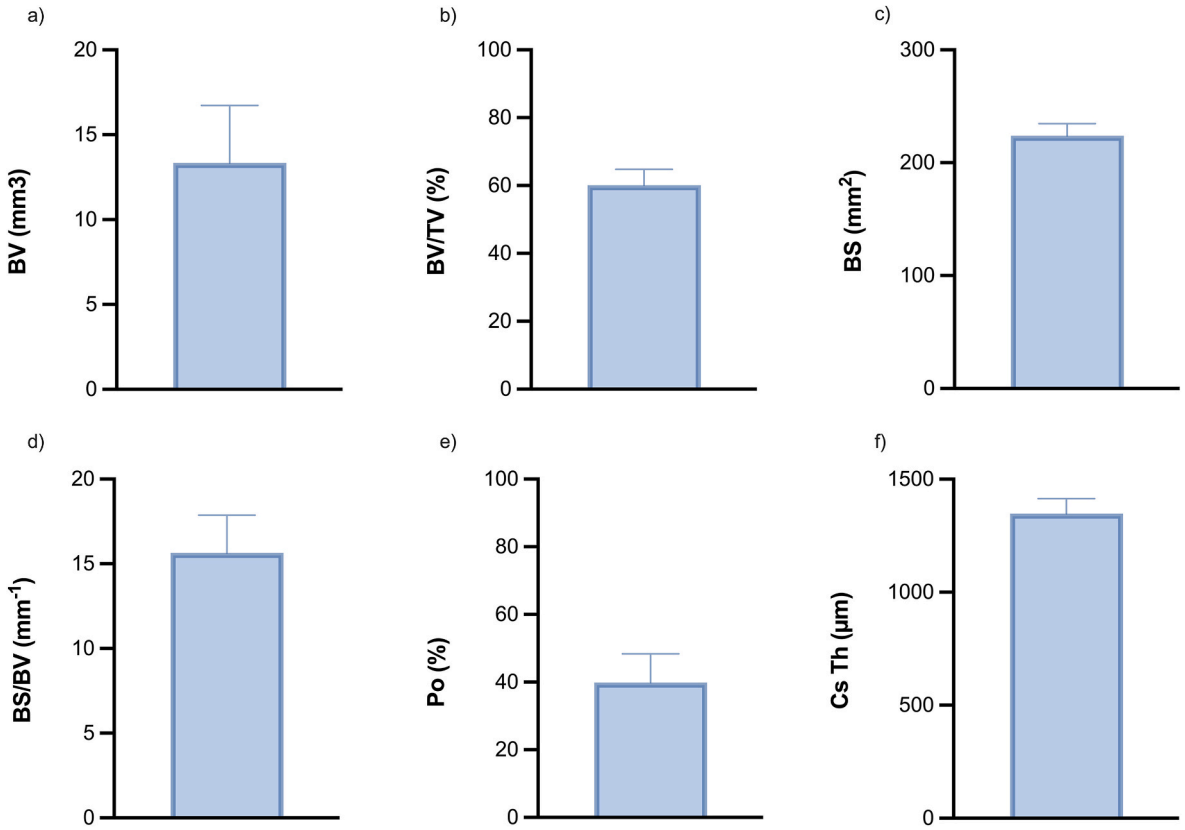

Fig. 6. Column bar charts of morphometric measures determined with micro-CT (voxel size 8.9 μm). Error bars indicate interquartile range. BV, total bone volume; BV/TV, bone volume fraction; BS, total bone surface; BS/BV, specific bone surface; Po(tot), total porosity percentage; Cs.Th, cross-sectional thickness.

Table 1
Comparison of morphometric parameters obtained by dental CBCT (voxel size 90 μm, slice thickness 90 μm) and resampled micro-CT (voxel size 90 μm, slice thickness 90 μm). IQR, interquartile range; BV, bone volume; BV/TV, bone volume fraction; BS, total bone surface; BS/BV, specific bone surface; Po, total porosity percentage; CsTh, cross-sectional thickness.

Morphometric parameters	Dental CBCT	Micro-CT (90 μm)	Wilcoxon	Spearman's
	Median [IQR]	Median [IQR]	p	ρ (p)
BV (mm^3)	15.68 [3.49]	14.52 [5.15]	0.470	0.972 (<0.001)
BV/TV (%)	68.96 [15.03]	66.70 [13.64]	0.133	0.783 (0.003)
BS (mm^2)	84.60 [23.55]	137.72 [31.66]	0.001	0.713 (0.009)
BS/BV (mm^{-1})	4.82 [1.52]	8.57 [3.67]	0.001	0.594 (0.042)
Po (%)	31.05 [15.03]	33.30 [13.64]	0.133	0.783 (0.003)
CsTh (μm)	1373 [220]	1411 [191]	0.356	0.951 (<0.001)

95% limits of agreement (LoA) surpassing the X-axis, suggesting strong agreement between the measurement instruments. BV/TV_{CBCT} was overestimated (bias 4.25%), while BS_{CBCT} (bias −51.05 mm^2) BS/BV_{CBCT} (−3.37 mm^{-1}), Po_{CBCT} (−4.25%) and $CsTh_{CBCT}$ (−38 μm) were underestimated.

3.4. C-arm CT measurements (voxel size 50 μm)

The RMSE of C-arm CT image registration was 0.1706 ± 0.1362 mm. The selected lower grey value threshold for image segmentation across all samples ranged between 120 and 190, individual values are reported in the appendix.

Significant differences were found between C-arm CT and 50 μm micro-CT mean BS and BS/BV ($p < 0.001$). Moreover, the difference between Po measurements was at the limit of statistical significance ($p = 0.050$). Mean BV, BV/TV and CsTh were not significantly different between C-arm CT and 50 μm micro-CT (Table 2). Strong and statistically significant correlations between C-arm CT and 50 μm micro-CT were found for all morphometric measures of interest ($\rho > 0.705$, $p \leq 0.010$) (Fig. 8). Bland-Altman analysis indicated strong agreement with 50 μm micro-CT measurements for $BV_{C\text{-}arm}$ (bias 0,27 mm^3), slight

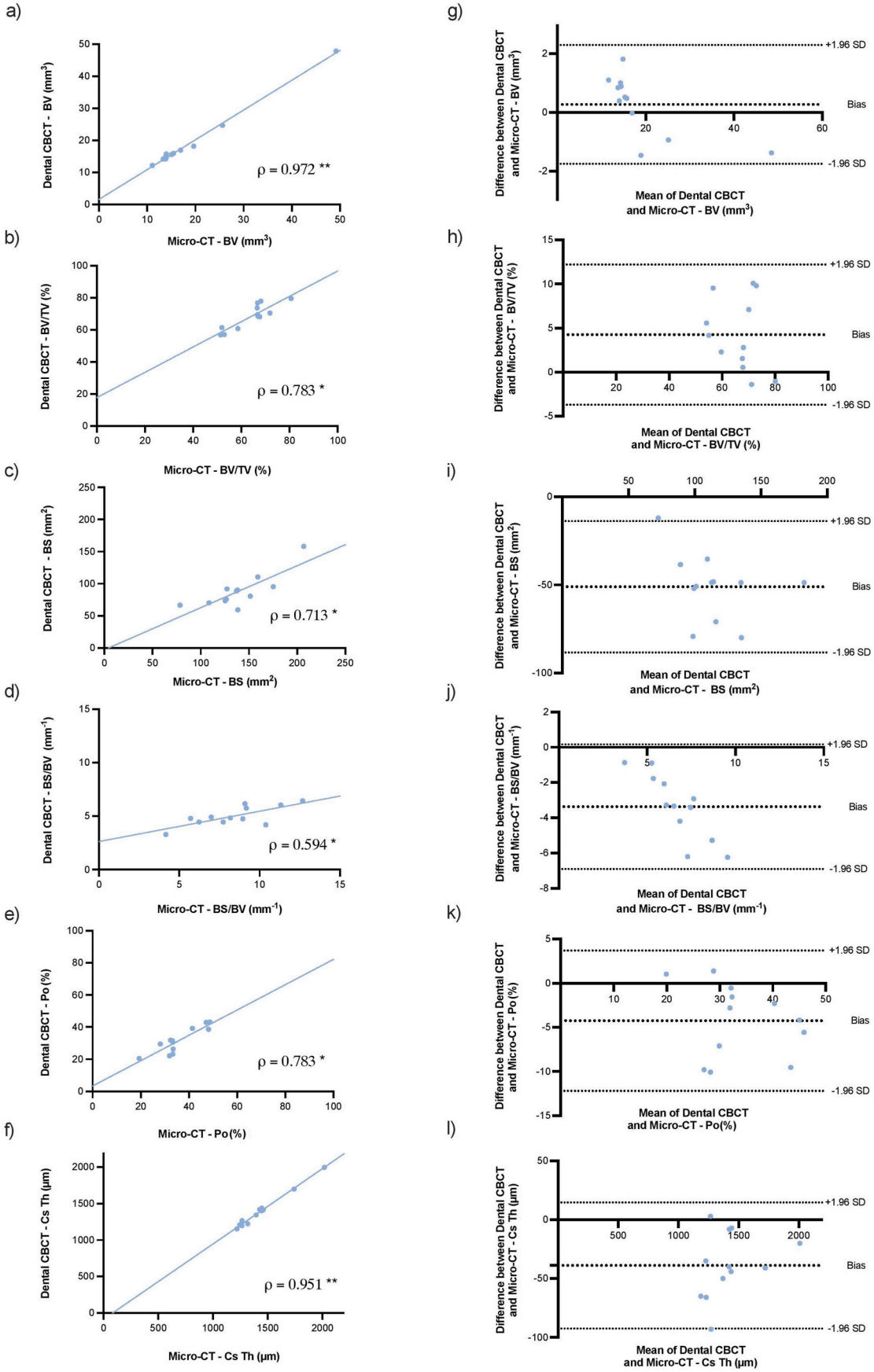

Fig. 7. Correlation between dental CBCT and 90 µm micro-CT measurements illustrated using scatter plots with Spearman correlation coefficients (a–f) and Bland-Altman plots (g–l). *p < 0.05, **p < 0.001.

Table 2
Comparison of morphometric parameters obtained by C-arm CT (voxel size 50 μm, slice thickness 100 μm) and resampled micro-CT (voxel size 50 μm, slice thickness 100 μm). IQR, interquartile range; BV, bone volume; BV/TV, bone volume fraction; BS, total bone surface; BS/BV, specific bone surface; Po, total porosity percentage; CsTh, cross-sectional thickness.

Morphometric parameters	C-arm CT	Micro-CT (50 μm)	Wilcoxon	Spearman's
	Median [IQR]	Median [IQR]	p	ρ (p)
BV (mm^3)	7.80 [6.14]	7.29 [5.44]	0.525	0.860 (<0.001)
BV/TV (%)	73.01 [13.17]	64.09 [17.19]	0.043	0.881 (<0.001)
BS (mm^2)	55.41 [27.11]	81.34 [30.89]	<0.001	0.706 (0.010)
BS/BV (mm^{-1})	6.11 [1.59]	11.35 [3.86]	<0.001	0.776 (0.003)
Po (%)	27.00 [13.17]	35.92 [17.19]	0.050	0.881 (<0.001)
CsTh (μm)	1298 [218]	1356 [196]	0.341	0.965 (<0.001)

overestimation of $BV/TV_{C\text{-}arm}$ (bias 8.01%) and underestimation of $BS_{C\text{-}arm}$ (bias −35.63 mm^2), $BS/BV_{C\text{-}arm}$ (bias −4.41 mm^{-1}), $Po_{C\text{-}arm}$ (bias −8.01%) and $CsTh_{C\text{-}arm}$ (bias −77.75 μm). In addition, a positive correlation between $BS_{\mu CT}$ and degree of underestimation of $BS_{C\text{-}arm}$ and $BS/BV_{C\text{-}arm}$ was observed.

3.5. Relation between morphometric measures and surgical outcomes

In the quest to identify an imaging biomarker predictive of spring-assisted surgery outcomes for CS, all morphometric measures were examined for potential correlations with postoperative CI. Only the SAC subgroup (n = 10) was included in this analysis, as SAC and SA-PVE have opposing effects on the CI. Furthermore, the sample size (n = 2) of the SA-PVE subgroup did not allow for a separate analysis. The aim of SA-PVE is to decrease the CI in children with a brachycephalic head shape, whereas an increase in CI is expected after SAC. Within the SAC subgroup, more complicated cases (n = 3) underwent pre-operative CT imaging of the skull, while conventional X-ray imaging was performed for uncomplicated cases (n = 7). Postoperatively all patients underwent conventional X-ray imaging. Three patients from the SAC subgroup were excluded due to insufficient quality of either pre-op or post-op imaging. A total of seven patients were included in this analysis; two had pre-op CT scans and five had pre-op X-rays. The Shapiro-Wilk test indicated a parametric distribution of pre- and postoperative CI values. Mean CI increased from 67.1 ± 2.8% pre-SAC to 71.4 ± 3.5% post-SAC ($p = 0.034$). The mean relative CI increase was 6.8 ± 3.4%, ranging between 2.1 and 11.0% (Fig. 9). Time interval between pre-operative imaging and SAC was not consistent between patients due to referral delays and waiting time for surgical treatment and ranged from 116 days to 0 days before SAC.

Strong and significant negative correlations with CI increase were found for $CsTh_{\mu CT}$ and $CsTh_{C\text{-}arm}$ ($\rho = -0.857$, $p = 0.014$) (Fig. 10). $CsTh_{CBCT}$ was not significantly associated with CI increase ($\rho = -0.393$, $p = 0.383$). Furthermore, significant correlations with CI increase were demonstrated for $BV_{\mu CT50}$ ($\rho = -0.857$, $p < 0.001$), $BV_{\mu CT90}$ ($\rho = -0.679$, $p = 0.008$) and BV_{CBCT} ($\rho = -0.643$, $p = 0.013$). It should be noted that the strength of correlation declined as micro-CT voxel size exceeded 50 μm. A negative trend with CI increase was found for $BV_{\mu CT}$ ($\rho = -0.679$, $p = 0.094$) and $BV_{C\text{-}arm}$ ($\rho = -0.652$, $p = 0.063$), but statistical significance could not be demonstrated.

In addition, significant correlations with CI increase were found for BS_{CBCT} ($\rho = -0.821$, $p < 0.001$) and BS/BV_{CBCT} ($\rho = -0.571$, $p = 0.033$). None of the other morphometric indices of interest showed correlation with postoperative CI increase. Furthermore, patient age at time of spring insertion was not significantly correlated to CI increase ($\rho = -0.481$, $p = 0.272$).

3.6. Comparison of radiation dose

The median dose area product (DAP) for C-arm CT and dental CBCT imaging was 462 ± 112 mGy/cm2 and 713 ± 0.8 mGy/cm2 respectively. In contrast, median DAP for conventional X-ray imaging of the skull, consisting of an AP and lateral view, was 284 ± 140 mGy/cm2. A total of five patients included in the present study underwent pre-operative helical CT scanning of the skull due to complicated sagittal CS or multi-sutural CS. The median dose length product (DLP) of helical CT imaging was 300 ± 242 mGy/cm.

4. Discussion

The aim of this study was to assess the reliability of clinically available CT modalities to measure calvarial bone microstructural properties in CS patients, and correlate these measurements with post-surgery head shape normalisation. Imaging biomarkers are needed to identify patients that will likely benefit from minimally invasive, spring-assisted surgery and exclude those at an increased risk of needing secondary calvarial remodelling.

In recent years numerous studies have investigated the use of CBCT for bone microstructure assessment (Guha et al., 2020; Van Dessel et al., 2013, 2016, 2017; Parsa et al., 2015). The majority have focused on dental applications, such as the assessment of alveolar bone quality prior to insertion of orthodontic implants. Although outcomes have not been entirely consistent, a trend of significant correlation between CBCT and micro-CT morphological measurements has been reported. In a series of three publications, Van Dessel et al. examined the ability of several CBCT devices to assess trabecular and cortical morphology of human mandibular bone (Van Dessel et al., 2013, 2016, 2017). Spatial resolution of CBCT devices ranged between 80 and 130 μm. The analysis demonstrated high overall reliability of morphometric indices calculation (ICC 0.62–0.99). Bone quantity-related measurements such as BV/TV and trabecular thickness (TbTh) were overestimated with CBCT, while the trabecular structural pattern remained similar. Overestimation of bone volume due to a lower image resolution is the result of a known artefact of CT-imaging called partial volume averaging. This occurs when materials of different densities, such as trabecular bone and air, occupy the same voxel. The grey value assigned to each voxel represents the average of the densities of materials within that voxel (Abel et al., 2013). As a result, a lower imaging resolution with larger voxel sizes will lead to an overestimation of total bone volume. In the present study, a slight overestimation of BV/TV was found with 90 μm dental CBCT ($\rho = 0.783$ ($p = 0.003$), bias 4.25%) and 50 μm C-arm CT imaging ($\rho = 0.881$ ($p < 0.001$), bias 8.01%). In contrast, both dental CBCT ($\rho = 0.972$ ($p < 0.001$) and bias 0.28 mm^3) and C-arm CT ($\rho = 0.860$ ($p < 0.001$) and bias 0.27 mm^3) did not overestimate BV.

Moreover, CBCT imaging has been reported to underestimate bone surface. Fine trabecular structures within human cancellous bone have a diameter below CBCT voxel size and can therefore not be visualized properly with CBCT. Kim et al. reported that BS was underestimated with CBCT imaging (voxel size 100 μm) when compared to micro-CT imaging at a voxel size of 96.87 μm ($r = 0.301$), and that underestimation was more severe when CBCT measurements were compared to micro-CT imaging at a voxel size of 19.37 μm ($r = 0.268$) (Kim et al., 2015). In the present study a similar trend of BS underestimation using CBCT ($\rho = 0.713$ ($p = 0.009$), bias −51.05 mm^2) and C-arm CT ($\rho = 0.706$ ($p = 0.010$), bias −35.63 mm^2) was found in comparison to micro-CT.

Limits of agreement and bias figures have to be interpreted in a clinical context to determine whether they are acceptable. The extent of measurement error that can be tolerated is different depending on the particular purpose for which the measurements are needed. It is difficult to state the exact limits of agreement that are acceptable for bone

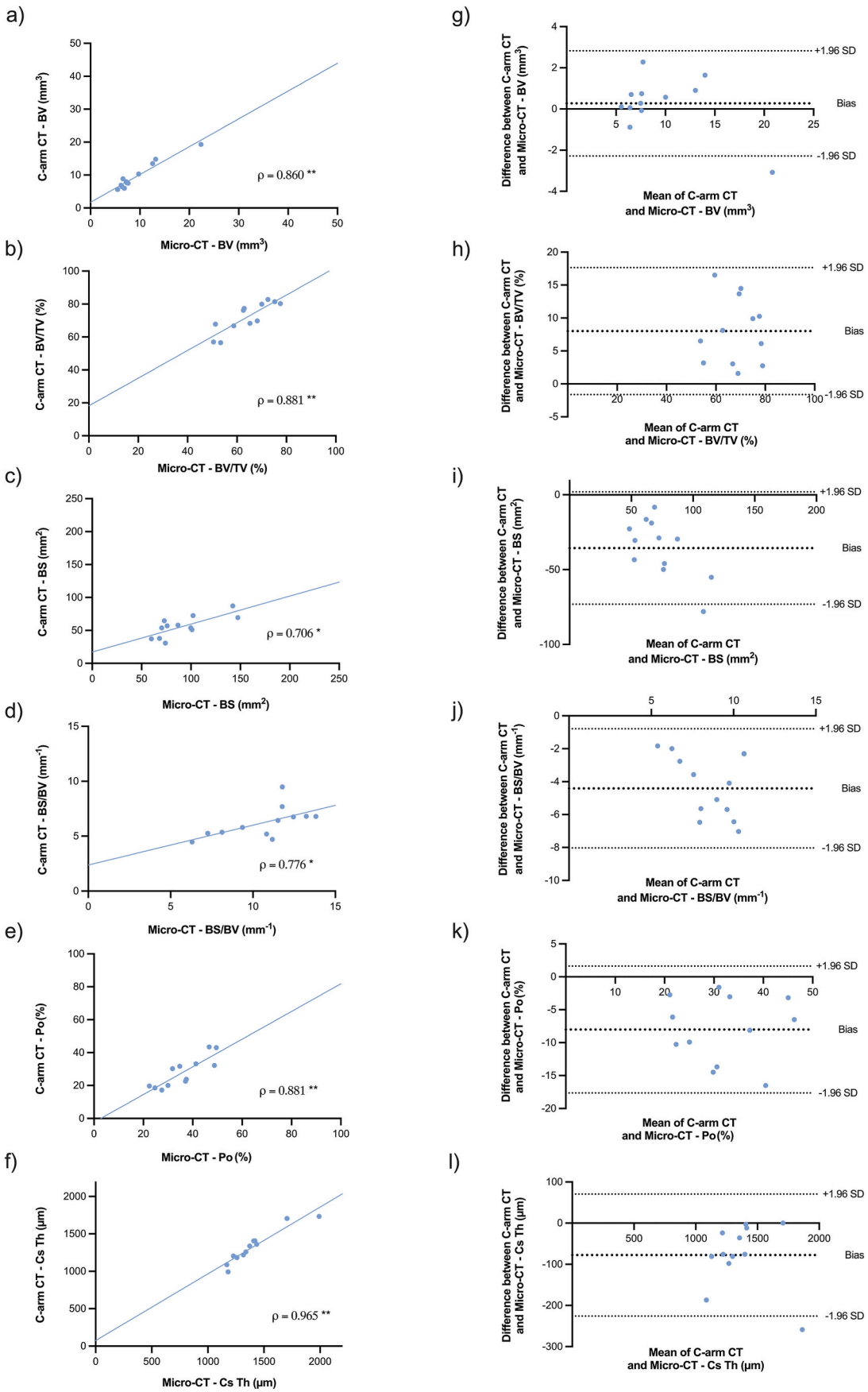

Fig. 8. Correlation between C-arm CT and 50 µm micro-CT measurements illustrated using scatter plots with Spearman correlation coefficients (a–f) and Bland-Altman plots (g–l). *p < 0.05, **p < 0.001.

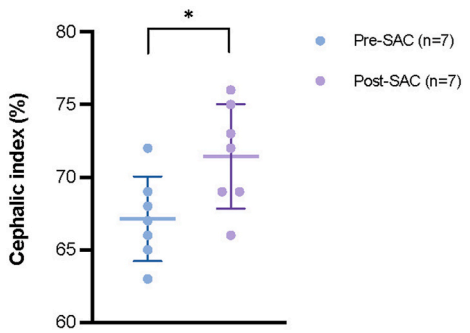

Fig. 9. Boxplots representing mean CI before and after SAC. Error bars indicate SD. CI was significantly higher after SAC (*p = 0.034).

microstructure assessment. The most important consideration is that morphometric parameters can be measured with sufficient reliability to preserve correlations with surgical outcomes.

To identify an imaging biomarker predictive of spring-assisted surgery outcome for CS, the relation between bone microstructural measurements and post-op CI was evaluated. Previous research has suggested that bone cross-sectional thickness is associated with CI changes after SAC. Based on assessment of both unilaminar and trilaminar samples, Rodriguez-Florez et al. reported that trilaminar structure in calvarium was associated with increased bone CsTh, and that trilaminar parietal bones were related to smaller changes in CI after SAC (Rodriguez-Florez et al., 2017). More detailed assessment of the relation between CsTh in trilaminar bone and surgical outcomes has not previously been investigated. Among all seven isolated CS patients included in this analysis, SAC led to an increase in CI with mean CI values rising from 67.1% pre-op to 71.4% immediately post-op. Our findings align with previous studies, which reported similar increases in CI ranging from 66.8-70% pre-op to 73–75.4% at spring removal (Rodriguez-Florez et al., 2017; Tenhagen et al., 2016; David et al., 2010; van Veelen and Mathijssen, 2012). The difference between CI immediately post-op in the present study and CI at spring removal in previous studies is likely due to the continuous and gradual nature of spring-induced expansion in the months after SAC.

In the present study significant, negative correlation to post-surgery CI increase was demonstrated for $CsTh_{C\text{-}arm}$ ($\rho = -0.857$, $p = 0.014$), $CsTh_{\mu CT}$ ($\rho = -0.857$, $p = 0.014$), $CsTh_{\mu CT50}$ ($\rho = -0.857$, $p < 0.001$) and $CsTh_{\mu CT90}$ ($\rho = -0.679$, $p = 0.008$). This indicates that even after calvarial bone develops to a three-layered structure, further increase in CsTh and decline of skull malleability leads to less successful outcomes after SAC. Although not significant, a negative trend with CI increase was observed for $CsTh_{CBCT}$ ($\rho = -0.679$, $p = 0.094$). This is likely caused by the inferior spatial resolution of dental CBCT (90 μm) in the present study compared to C-arm CT (50 μm). Another morphometric measure we found correlated to postoperative CI changes is BV. $BV_{\mu CT50}$ ($\rho = -0.857$, $p < 0.001$), $BV_{\mu CT90}$ ($\rho = -0.679$, $p = 0.008$) and BV_{CBCT} ($\rho = -0.643$, $p = 0.013$) were significantly, negatively correlated to CI increase. In addition, negative trends were found for $BV_{\mu CT}$ ($\rho = -0.679$, $p = 0.094$) and $BV_{C\text{-}arm}$ ($\rho = -0.652$, $p = 0.063$). Based on the current results, C-arm CT appears most promising for calculating pre-operative morphometric indices. Further research should be conducted to validate CsTh and BV as biomarkers for post-surgery CI increase.

An important consideration when subjecting patients to radiological examinations is potential harm due to exposure to ionising radiation. Because of their long life expectancy post-exposure and developing bodies with a high rate of cell division, this is especially a concern in children. In a retrospective cohort study among 178,604 patients in Great Brittain who underwent CT-imaging before the age of 22, Pearce et al. reported an excess relative risk of developing leukaemia (0.036 per mGy, 95% CI 0.005–0.120, $p = 0.0097$) and brain tumours (0.023 per mGy, 95% CI 0.010–0.049, $p < 0.0001$) compared to the general population (Pearce et al., 2012). In the present study, median DAP for dental CBCT, C-arm CT and skull X-ray imaging were 713 ± 0.8, 462 ± 112 and 284 ± 140 mGy/cm^2, respectively. In contrast, median DLP for pre-operative helical CT imaging of the skull due to complicated sagittal CS or multi-sutural CS was 300 ± 242 mGy/cm. Since DLP is a measure of radiation output rather than absorbed radiation dose, it would have to be adjusted for patient head size to obtain a value that is comparable to DAP. The smallest BPD among the patients included in the present study was 8.6 cm. Based on this information, it can be stated that a helical CT scan of the skull exposes the patient to a radiation dose in magnitude of CBCT and conventional X-ray imaging (Rehani and Berry, 2000; Samelson et al., 2019). This is in line with commonly reported radiation exposure figures for helical CT imaging. For instance, CT imaging of the chest is known to give a radiation exposure equivalent to 400 chest radiographs. The relatively minor radiation dose of CBCT imaging seems acceptable considering the benefit of bone microstructure assessment in pre-surgical planning.

This preliminary study was limited to in-vitro examination of bone specimens and did not consider the influence of soft tissue on image resolution. In-vivo validation of bone microstructure assessment using CBCT is required before results can be translated to clinical practice. Furthermore, only samples with a trilaminar structure were included. Now that correlation between CBCT and micro-CT imaging has been demonstrated in trilaminar samples, future research should investigate CBCT assessment of bone microstructure in unilaminar samples. Sample size in the present study was limited (n = 12). Although correlation between imaging modalities and relation with surgical outcomes was statistically significant for several morphometric parameters, increased sample size would improve statistical accuracy. Power analysis based on current results (BV/TV and BS/BV measurements of C-arm CT and 50 μm micro-CT) suggest a sample size of 32 bone specimens assuming 90% power with an alpha of 0.05.

Moreover, manual image segmentation is likely to have induced a degree of operator dependency. Accurate image segmentation is a necessity for reliable morphometric analysis of the bone. Grey value tresholds are selected to separate bone from non-bone and create a binarized image. As image resolution decreases, identifying the optimal threshold becomes more challenging. In the present study, lower grey value thresholds were operator-selected per bone sample. Binarized images were visually validated to confirm the most accurate segmentation overlap with the original image. Lastly, CI was the sole parameter used to evaluate postoperative head shape changes. Although commonly used as a surgical outcome measure, CI has been criticised for only assessing the scaphocephalic skull on a two-dimensional level and not considering dysmorphological features such as frontal bossing and occipital prominence (Tenhagen et al., 2016; David et al., 2010; Skadorwa et al., 2024). Novel scaphocephaly severity indices have been introduced in recent years that attempt to reflect head shape changes on a three-dimensional level and include assessment of frontal and occipital malformations. However, translation of novel scaphocephaly severity indices to clinical practice has proven challenging as they are often time-consuming and require 3D CT imaging of the skull, which is not routinely performed for uncomplicated sagittal CS. For the time being, CI remains the most practical measure to quantify surgical outcomes for scaphocephaly in daily clinical practice.

5. Conclusion

The present study demonstrates the potential of clinical CT devices (dental CBCT and C-arm CT) for the assessment of calvarial bone microstructure in craniosynostosis patients, to aid in pre-surgical decision making. Because of its possible use in theatre settings and relatively high imaging resolution with a voxel size of 50 μm, C-arm CT appears most promising for this purpose. Parietal bone thickness and bone volume appear to be suitable imaging biomarkers to predict head shape changes following SAC. Further research is needed to evaluate CBCT

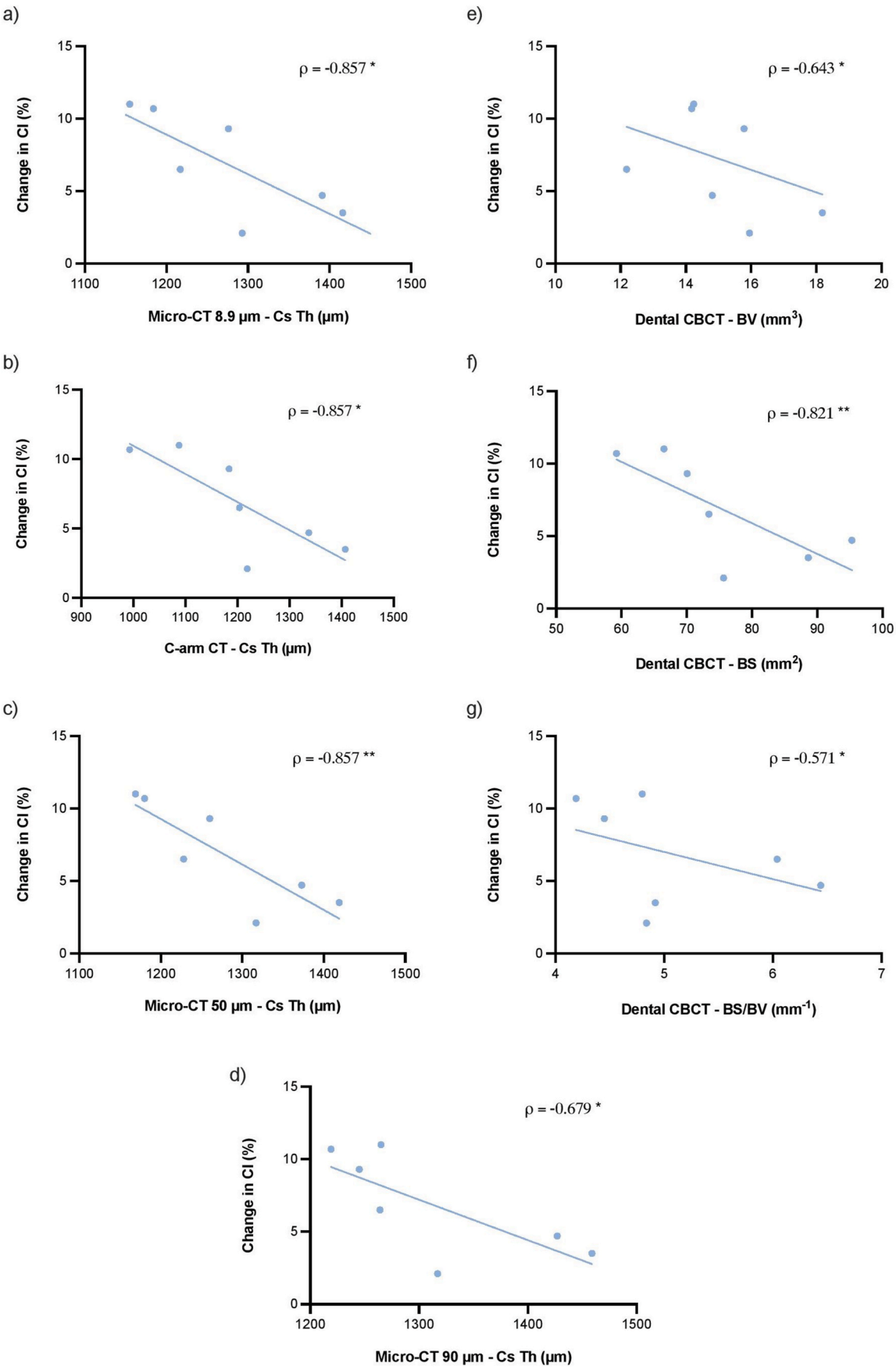

Fig. 10. Significant correlations between 8.9 µm micro-CT CsTh (a), C-arm CT CsTh (b), 50 µm micro-CT CsTh (c), 90 µm micro-CT CsTh (d), dental CBCT BV, dental CBCT BS (f) and dental CBCT BS/BV (g) with CI increase after SAC. *$p < 0.05$, **$p < 0.01$.

microstructure assessment in unilaminar calvarial bone and validate its use in-vivo.

Informed consent

Parental consent was obtained prior to surgery.

Ethics approval

This study was approved by the UK Health Research Authority (REC reference 09/H0722/28).

Declaration of competing interest

The authors declare to have no conflict of interest.

Acknowledgements

The work has been funded by Great Ormond Street Hospital for Children Charity (grant number 12SG15) as well as the NIHR British Research Council Advanced Therapies for Structural Malformations and Tissue Damage pump-prime funding call (grant n. 17DS18), the Great Ormond Street Hospital Charity Clinical Research Starter Grant (grant n. 17DD46) and the European Research Council (ERC-2017-StG- 757923). This report incorporates independent research from the National Institute for Health Research Biomedical Research Centre Funding Scheme. The views expressed in this publication are those of the author(s) and not necessarily those of the NHS, the National Institute for Health Research or the Department of Health.

APPENDIX

Table A
Selected lower grey value threshold for image segmentation

Sample	Micro-CT	Dental CBCT	C-arm CT
P29	55	180	157
P46	55	180	140
P49	55	180	140
P50	55	175	120
P51	55	185	145
P52	55	140	150
P56	55	165	145
P60	55	150	190
P69	55	150	160
P88	55	150	142
P125	55	185	150
P126	55	170	147

* Upper grey value threshold was consistent at 255 for every sample.

Table B
RMSE of image registration

Sample	Dental CBCT	C-arm CT
	RMSE (mm)	RMSE (mm)
P29	0.1699	0.1770
P46	0.1955	0.0000
P49	0.2559	0.2847
P50	0.2531	0.2236
P51	0.1720	0.0000
P52	0.2481	0.1187
P56	0.1448	0.2026
P60	0.1740	0.0392
P69	0.1992	0.3418
P88	0.1370	0.3983
P125	0.1975	0.0000
P126	0.3420	0.2608
Mean RMSE	**0.2074**	**0.1706**

References

Abel, R., Prime, M., Jin, A., Cobb, J., Bhattacharya, R., 2013. 3D imaging bone quality: bench to bedside. Hard Tissue 2.

Ajami, S., Rodriguez-Florez, N., Ong, J., Jeelani, NuO., Dunaway, D., James, G., et al., 2022. Mechanical and morphological properties of parietal bone in patients with sagittal craniosynostosis. J. Mech. Behav. Biomed. Mater. 125, 104929.

Bland, J.M., Altman, D.G., 1995. Comparing methods of measurement: why plotting difference against standard method is misleading. Lancet 346 (8982), 1085–1087.

Breakey, R.W.F., van de Lande, L.S., Sidpra, J., Knoops, P.M., Borghi, A., O'Hara, J., et al., 2021. Spring-assisted posterior vault expansion-a single-centre experience of 200 cases. Childs Nerv Syst. 37 (10), 3189–3197.

Dach, E., Bergauer, B., Seidel, A., von Wilmowsky, C., Adler, W., Lell, M., et al., 2018. Impact of voxel size and scan time on the accuracy of three-dimensional radiological imaging data from cone-beam computed tomography. J. Cranio-Maxillo-Fac. Surg. 46 (12), 2190–2196.

David, L.R., Plikaitis, C.M., Couture, D., Glazier, S.S., Argenta, L.C., 2010. Outcome analysis of our first 75 spring-assisted surgeries for scaphocephaly. J. Craniofac. Surg. 21 (1), 3–9.

Donnelly, E., 2011. Methods for assessing bone quality: a review. Clin. Orthop. Relat. Res. 469 (8), 2128–2138.

Guha, I., Klintstrom, B., Klintstrom, E., Zhang, X.L., Smedby, O., Moreno, R., et al., 2020. A comparative study of trabecular bone micro-structural measurements using different CT modalities. Phys. Med. Biol. 65 (23), 14.

Ibrahim, N., Parsa, A., Hassan, B., van der Stelt, P., Aartman, I.H.A., Wismeijer, D., 2014. Accuracy of trabecular bone microstructural measurement at planned dental implant sites using cone-beam CT datasets. Clin. Oral Implants Res. 25 (8), 941–945.

Ibrahim, N., Parsa, A., Hassan, B., van der Stelt, P., Rahmat, R.A., Ismail, S.M., et al., 2021. Comparison of anterior and posterior trabecular bone microstructure of human mandible using cone-beam CT and micro CT. BMC Oral Health 21 (1), 6.

Kim, J.E., Yi, W.J., Heo, M.S., Lee, S.S., Choi, S.C., Huh, K.H., 2015. Three-dimensional evaluation of human jaw bone microarchitecture: correlation between the microarchitectural parameters of cone beam computed tomography and micro-computer tomography. Oral Surg Oral Med Oral Pathol Oral Radiol 120 (6), 762–770.

Klintström, E., Smedby, O., Moreno, R., Brismar, T.B., 2014. Trabecular bone structure parameters from 3D image processing of clinical multi-slice and cone-beam computed tomography data. Skeletal Radiol. 43 (2), 197–204.

Klintström, E., Klintström, B., Moreno, R., Brismar, T.B., Pahr, D.H., Smedby, Ö., 2016. Predicting trabecular bone stiffness from clinical cone-beam CT and HR-pQCT data; an in vitro study using finite element analysis. PLoS One 11 (8), e0161101.

Kulah, K., Gulşahi, A., Kamburoğlu, K., Geneci, F., Ocak, M., Celik, H.H., et al., 2019. Evaluation of maxillary trabecular microstructure as an indicator of implant stability by using 2 cone beam computed tomography systems and micro-computed tomography. Oral Surg Oral Med Oral Pathol Oral Radiol 127 (3), 247–256.

Manske, S., Macdonald, H., Nishiyama, K., Boyd, S., McKay, H., 2010. Clinical tools to evaluate bone strength. Clin. Rev. Bone Miner. Metabol. 8, 122–134.

Mys, K., Stockmans, F., Vereecke, E., van Lenthe, G.H., 2018. Quantification of bone microstructure in the wrist using cone-beam computed tomography. Bone 114, 206–214.

Mys, K., Varga, P., Stockmans, F., Gueorguiev, B., Neumann, V., Vanovermeire, O., et al., 2021. High-resolution cone-beam computed tomography is a fast and promising technique to quantify bone microstructure and mechanics of the distal radius. Calcif. Tissue Int. 108 (3), 314–323.

Orth, R.C., Wallace, M.J., Kuo, M.D., 2008. C-arm cone-beam CT: general principles and technical considerations for use in interventional radiology. J. Vasc. Intervent. Radiol. 19 (6), 814–820.

Parsa, A., Ibrahim, N., Hassan, B., van der Stelt, P., Wismeijer, D., 2015. Bone quality evaluation at dental implant site using multislice CT, micro-CT, and cone beam CT. Clin. Oral Implants Res. 26 (1), e1–e7.

Pearce, M.S., Salotti, J.A., Little, M.P., McHugh, K., Lee, C., Kim, K.P., et al., 2012. Radiation exposure from CT scans in childhood and subsequent risk of leukaemia and brain tumours: a retrospective cohort study. Lancet 380 (9840), 499–505.

Rehani, M.M., Berry, M., 2000. Radiation doses in computed tomography. The increasing doses of radiation need to be controlled. BMJ 320 (7235), 593–594.

Rodgers, W., Glass, G.E., Schievano, S., Borghi, A., Rodriguez-Florez, N., Tahim, A., et al., 2017. Spring-assisted cranioplasty for the correction of nonsyndromic scaphocephaly: a quantitative analysis of 100 consecutive cases. Plast. Reconstr. Surg. 140 (1), 125–134.

Rodriguez-Florez, N., Ibrahim, A., Hutchinson, J.C., Borghi, A., James, G., Arthurs, O.J., et al., 2017. Cranial bone structure in children with sagittal craniosynostosis: relationship with surgical outcomes. J. Plast. Reconstr. Aesthetic Surg. 70 (11), 1589–1597.

Samelson, E.J., Broe, K.E., Xu, H., Yang, L., Boyd, S., Biver, E., et al., 2019. Cortical and trabecular bone microarchitecture as an independent predictor of incident fracture risk in older women and men in the Bone Microarchitecture International Consortium (BoMIC): a prospective study. Lancet Diabetes Endocrinol. 7 (1), 34–43.

Skadorwa, T., Wierzbieniec, O., Podkowa, K., Sośnicka, K., 2024. The validation of morphometric outcomes and stratification system for nonsyndromic sagittal craniosynostosis following total calvarial remodeling. J. Cranio-Maxillo-Fac. Surg. 52 (10), 1148–1154.

Tenhagen, M., Bruse, J.L., Rodriguez-Florez, N., Angullia, F., Borghi, A., Koudstaal, M.J., et al., 2016. Three-dimensional handheld scanning to quantify head-shape changes in spring-assisted surgery for sagittal craniosynostosis. J. Craniofac. Surg. 27 (8), 2117–2123.

Van Dessel, J., Huang, Y., Depypere, M., Rubira-Bullen, I., Maes, F., Jacobs, R., 2013. A comparative evaluation of cone beam CT and micro-CT on trabecular bone structures in the human mandible. Dentomaxillofacial Radiol. 42 (8), 20130145.

Van Dessel, J., Nicolielo, L.F.P., Huang, Y., Slagmolen, P., Politis, C., Lambrichts, I., et al., 2016. Quantification of bone quality using different cone beam computed tomography devices: accuracy assessment for edentulous human mandibles. Eur. J. Oral Implant. 9 (4), 411–424.

Van Dessel, J., Nicolielo, L.F., Huang, Y., Coudyzer, W., Salmon, B., Lambrichts, I., et al., 2017. Accuracy and reliability of different cone beam computed tomography (CBCT) devices for structural analysis of alveolar bone in comparison with multislice CT and micro-CT. Eur. J. Oral Implant. 10 (1), 95–105.

van Veelen, M.L., Mathijssen, I.M., 2012. Spring-assisted correction of sagittal suture synostosis. Childs Nerv Syst. 28 (9), 1347–1351.

Wang, F., Zheng, L., Theopold, J., Schleifenbaum, S., Heyde, C.E., Osterhoff, G., 2022. Methods for bone quality assessment in human bone tissue: a systematic review. J. Orthop. Surg. Res. 17 (1), 174.